Photodoping-Driven Crossover in the Low-Frequency Noise of MoS_2 Transistors

Isidoro Martinez,[1] Mário Ribeiro,[2] Pablo Andres,[1] Luis E. Hueso,[2,3] Fèlix Casanova,[2,3,*] and Farkhad G. Aliev[1,†]

[1]*Departamento Fisica Materia Condensada, C03, Instituto Nicolas Cabrera (INC), Condensed Matter Physics Institute (IFIMAC), Universidad Autonoma de Madrid, 28049 Madrid, Spain*

[2]*CIC NanoGUNE, Donostia-San Sebastian 20018, Basque Country, Spain*

[3]*IKERBASQUE, Basque Foundation for Science, Bilbao 48013, Basque Country, Spain*

(Received 2 December 2016; revised manuscript received 24 February 2017; published 31 March 2017)

Transition-metal dichalcogenide field-effect transistors (FETs) have been actively explored for low-power electronics, light detection, and sensing. Albeit promising, their performance is strongly limited by low-frequency noise (LFN). Here, we report on the study of LFN in MoS_2 FETs on SiO_2 substrates in ambient conditions using photodoping. Using this external excitation source allows us to access different nonequilibrium steady states and cross over different noise regimes. We observe a dependence of the noise power spectrum on the transient decay time window, approaching $1/f$ type when the system is closer to equilibrium, and identify a dependence of the LFN on channel thickness. Monolayer and bilayer devices exhibit random telegraph noise for insulating regimes and $1/f$-type Hooge mobility fluctuations (HMFs) for conductive regimes. Thicker devices exhibit mainly $1/f$-type carrier-number fluctuations (CNFs). In the latter, we observe a photodoping-induced change from a near-parabolic to a near-linear dependence of the inverse $1/f$ noise amplitude above the threshold gate voltage. This change indicates a crossover in the LFN mechanism from CNFs to HMFs. We demonstrate that the study of conductance and noise under photodoping is an effective tool to identify dominating carrier noise mechanisms in few-atomic-layer FETs for a wide range of doping regimes.

DOI: 10.1103/PhysRevApplied.7.034034

I. INTRODUCTION

Collective wavelike fluctuations are ubiquitous and inherent to two-dimensional (2D) van der Waals (vdW) semiconductors, being responsible for nontrivial modifications of noncovalent interactions at the nanoscale [1]. In few-layer-thick 2D vdW electrical devices, the high surface-to-volume ratio and the ultimate thinness of the channel make conduction electrons particularly vulnerable to traps, ionized impurities, and changes in the scattering cross section. These fluctuations can manifest as low-frequency noise (LFN) with a power spectrum $S_I(f)$ closely following an inverse dependence with a frequency f, $1/f^{\beta}$, where β is a characteristic exponent. Although LFN dominates the power spectrum at low frequency, it is the main contributor to the phase noise of sensors and high-frequency operating systems due to its up-conversion to high frequencies [2]. For these reasons, LFN has emerged as a key limiting factor in the performance of 2D vdW-based devices, particularly under low-doping regimes [3–6]. It is thus crucial to understand the processes responsible for the fluctuation of the electrical current in such devices for future applications.

The unique electrical and optical properties of ultrathin films of transition-metal dichalcogenides (TMDs) have been intensively explored in few-atomic-layer field-effect transistors (FETs) [7,8]. MoS_2 FETs in particular have been actively investigated for low-power electronics [7,9,10], light detection, photocurrent generation [11–13], and sensing [14,15].

In MoS_2 FETs, the presence of trapping or detrapping processes at the channel-to-insulator and vacuum interfaces has been demonstrated to drive biexponential current relaxation [16], as well as time-dependent contributions to the electron-transport characteristics [17] and to differences in the carrier density. These processes contribute to the slow relaxation of the photoconductivity in MoS_2 [18]. In recent years, noise in monolayer-to-multilayer TMD FETs has been mainly described by carrier-number fluctuations (CNFs) [4,5,15,19–27], with some exceptional cases reporting phenomenological Hooge mobility fluctuations (HMFs) [3,25], where $1/f$ noise is interpreted in terms of the fluctuation of the free-path length of the charge carriers [28]. This percolative nature of the electron conduction has been shown to be a dominant noise mechanism in multilayer WSe_2 FETs [6,29]. Although CNF is seen as the dominant LFN mechanism in MoS_2, there is no clear explanation for the microscopic physical mechanisms behind noise in the cases where HMF has been observed. It is therefore worth investigating photodoping as an external stimulus to access different low-frequency noise regimes in a set of TMD FETs with different thicknesses.

Here, we present a study of electron transport and photoconductivity in monolayer-to-bulk MoS_2 FETs to address three important questions: (i) how transient decays affect LFN in backgated MoS_2 FETs, (ii) whether

*f.casanova@nanogune.eu
†farkhad.aliev@uam.es

photodoping, by modulating the charge carrier density, can change the LFN mechanisms, and (iii) if LFN mechanisms in MoS_2 FETs undergo a significant change with an incremental channel layer number. Furthermore, by providing an additional route to identify the physical mechanisms behind LFN in TMD FETs, we pave the road to the development of alternative approaches for optimizing TMD-based photodetectors and transistors.

II. EXPERIMENTAL DETAILS

We study four MoS_2 FET devices with monolayer, bilayer, trilayer, and bulklike MoS_2 channels, henceforth identified as devices I, II, III, and IV, respectively. The sample preparation is carried out using high-purity bulk MoS_2 crystals acquired from a commercially available supplier (SPI Supplies). The MoS_2 FETs are fabricated on n^+-doped silicon dies with thermally grown 250-nm-thick SiO_2. The substrates are cleaned and sonicated in acetone, isopropanol, and deionized water and dried on a hotplate at 195 °C. Following an all-dry viscoelastic-stamping deterministic-transfer procedure [30] using polydimethylsiloxane, MoS_2 flakes with different numbers of atomic layers are optically identified and selectively transferred onto the SiO_2 substrates. Standard electron-beam lithography using a double layer of polymethyl methacrylate (495/950 MDa) is employed to pattern Ti(5 nm)/Au(35 nm) metal contacts. The metallization is done in an ultrahigh-vacuum deposition system at a base pressure of 10^{-9} mbar, using electron-beam evaporation to deposit Ti and Au. The lift-off is performed in acetone. Figure 1(a) shows the sketch of the FET electrical configuration, with MoS_2 channel, SiO_2 (250 nm) dielectric, Si backgate, and Ti(5 nm)/Au(35 nm) contacts. Figure 1(b) shows a microscopic picture of device III.

The thickness of the MoS_2 flakes is determined using Raman spectroscopy with a 532-nm laser line at room temperature [see Fig. 1(c)]. The difference between the frequency of the Raman E^1_{2g} and A_{1g} peaks, $\Delta(A_{1g} - E^1_{2g})$, can be used as a reliable indicator of the number of layers of the flake [31]. The frequencies of the peaks are determined by using a double-Lorentzian least-squares best fit. The obtained $\Delta(A_{1g} - E^1_{2g})$ of 20.2, 22.8, 23.2, and 24.9 cm^{-1} are in agreement with the expected values for monolayers, bilayers, trilayers, and bulk, respectively. The lateral dimensions (length L and width W) of device I are $L = 3.7$ μm and $W = 2.8$ μm; of device II, $L = 3.6$ μm and $W = 4.3$ μm; of device III, $L = 5.6$ μm and $W = 5.5$ μm; and of device IV, $L = 52$ μm and $W = 12$ μm.

Because of the relatively high resistance of the MoS_2 FETs, both current and current noise are measured with a Keithley 6485 picoammeter. A homemade battery designed for ultralow noise at a bias of 1 V powers the voltage applied between the drain and the source contacts, while a gate voltage up to 80 V is applied between the substrate and the drain using a Keithley 228A voltage source. In the set of measurements performed during this study, the amplifier noise and the Johnson noise are orders of magnitude below the detected noise levels, which allows us to disregard spurious origins for the observed signals.

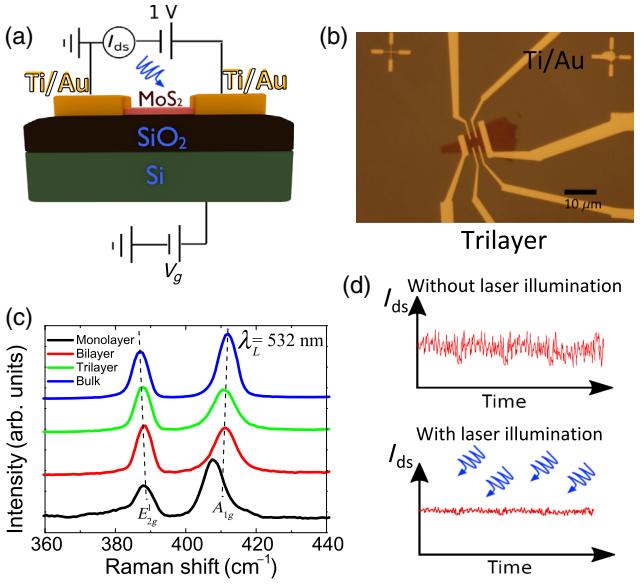

FIG. 1. (a) Sketch of the two-point measurement setup. The MoS_2 channel is contacted by Ti/Au contacts, with SiO_2 used as a backgate dielectric. The open top channel allows for the use of a photodoping technique. (b) Optical microscope image of the trilayer (device III) MoS_2 FET. Scale bar of 10 μm. (c) Raman spectra for the several devices explored in this work. The E^1_{2g} and A_{1g} labels identify the two vibrational modes used to determine the MoS_2 thickness. (d) Sketch showing the time dependence of drain-source current, I_{ds}, with and without laser illumination, indicating reduced normalized current noise power under laser illumination.

The current intensity time series are measured at every fixed gate for 180 s with a resolution of 67 ms. The FETs are illuminated with a TOPTICA-iBeam Smart diode laser with a wavelength of 487 nm and with up to 1 mW of nominal output power. The maximum effective light surface density is estimated to be substantially below 1 $\mu W/\mu m^2$. A laser spot approximately tens of micrometers in diameter covers the whole surface of the MoS_2 channel. All of the measurements are performed at room temperature and in ambient conditions. LFN experiments are carried out by studying the current relaxation time series after steeply sweeping up the gate voltage by 2 V under two different conditions: (i) dark conditions, where no laser illumination is applied, and (ii) in the presence of laser illumination. Figure 1(d) shows schematically how the normalized current noise varies under photodoping.

III. RESULTS AND DISCUSSION

A. Electron transport with and without photodoping

In the body of the manuscript, we concentrate mainly on the results obtained for devices II and III, between which a

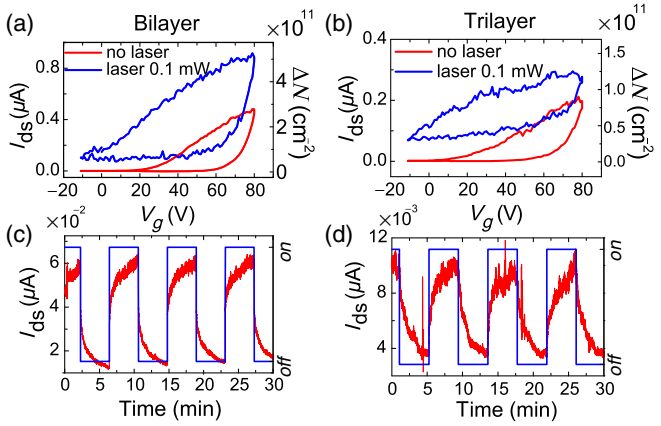

FIG. 2. Transfer characteristics of the drain-source current I_{ds} as a function of the gate voltage V_g with and without laser illumination of (a) device II and (b) device III. Gate-voltage sweep rate is 1 V/s. The right axes present the corresponding gate dependences of the photoexcited carrier concentrations (see the text for details). (c),(d) Laser pulse responses of the photocurrent for devices II and III, respectively, without applied V_g, and the applied drain-source bias V_{ds} of 1 V. Blue solid line represents the time dependence of the $on:off$ incidence of illumination with laser output power of 0.1 mW. The period $T = 500$ s.

significant change in the LFN under photodoping is observed. Some relevant complementary results for devices I and IV are provided in the Supplemental Material [32].

We start by evaluating the dc transport with and without illumination to establish a foot ground for the LFN studies. Figures 2(a) and 2(b) show the gate dependence of the drain-source current I_{ds} (transfer characteristics) with and without laser illumination. The nonilluminated FETs exhibit n-type behavior with on:off ratios of the order of 10^5–10^6. In agreement with previous reports [16,33], the transfer characteristics of devices II and III reveals hysteretic behavior due to current relaxation. Qualitatively similar effects are shown in Fig. 1S of the Supplemental Material [32] for devices I and IV. With laser illumination, the current output of the transistor *off* state greatly increases from 10^{-12} to 10^{-7} A, while the current output at the *on* state increases by a factor of 2. In both cases, the hysteretic behavior slightly increases, which is in line with previous studies [16].

Devices II and III exhibit maximum field-effect mobilities of 9 and 14 $cm^2/V\,s$, respectively. The field-effect mobilities of devices II and III are calculated from the expression $\mu_{FE} = Lg_m/(WC_{ox}V_{ds})$, where g_m is the terminal transconductance (dI_{ds}/dV_g) and C_{ox} the gate capacitance per unit area, estimated to be 1.38×10^{-4} F/m^2 for a 250-nm-thick SiO_2 dielectric, using a parallel-plate model. Ti/Au contacts to the MoS_2 channel provide low Schottky barriers of 0.05 eV [34], which, at room temperature, result in Ohmic-like output characteristics (see Fig. 2S in the Supplemental Material [32]).

Figures 2(c) and 2(d) show the drain-source photocurrent generated by a laser pulse of the period $T = 500$ s at zero gate voltage for devices II and III, respectively, under an applied drain-source bias, V_{ds}, of 1 V. Exponential-decay time constants of about 180 s are observed before reaching the equilibrium state, for both the *on* and *off* states of the laser illumination. Similar curves for devices I and IV are shown in Figs. 3S(a) and 3S(b) of the Supplemental Material [32]. The normalized variation of the pulsed photocurrent as a function of the MoS_2 channel thickness [see Fig. 3S(c) in the Supplemental Material [32]] points out the difference between devices with an increasing number of layers, with the maximum photocurrent response evident at two or three layers.

We estimate the additional photoexcited carrier density, ΔN, generated under illumination using a simplified relation between conductance, mobility, and carrier concentration, given by $\Delta\sigma \approx e(\mu_h \Delta N_h + \mu_e \Delta N_e)$, with $\Delta\sigma$ being the change in surface conductance, μ_h and μ_e the hole and electron mobilities, and ΔN_h, ΔN_e the change in hole and electron concentrations. Being n doped, we assume the presence of one type of carriers only (electrons) and that, for the minimum applied laser power (0.1 mW), the carrier-concentration change is larger than the change in the Hall mobility [35]. Figures 2(a) and 2(b) show the change in carrier density between dark and illuminated states for devices II and III.

B. Low-frequency noise without photodoping

We now turn to investigating how the LFN parameters change along the current relaxation. For this study, we use the determined exponential-decay time constant of about 180 s. Photocurrent relaxation of similar time scales has been reported for MoS_2 FETs [18], having been attributed to the presence of random potentials in the device due to defects. For the noise analysis, we divide the current time series (both in dark conditions and under illumination) into three periods, $P1$, $P2$, $P3$, each lasting for about 60 s. For each of these intervals, the noise power spectrum of the current is analyzed separately by using the Hooge relation [3,28], $S_I = [(\alpha I_{ds}^2)/f^\beta]$, where S_I is the square of the module of the fast Fourier transform of the current time series expressed as a function of the frequency f, the source-drain current I_{ds} is under equilibrium, and α and β are the characteristic Hooge parameters obtained from fits in the 0.05–5 Hz frequency range. When β is close to 1 (i.e., roughly between 0.7 and 1.5) the noise is usually called $1/f$ noise [28]. The strong dependence of the channel resistivity on gate voltage (with a change up to 6 orders of magnitude between the *on* and *off* states) requires that we fix the applied V_{ds} and record continuously I_{ds} flowing through the device for consecutively increasing gate-voltage steps of 2 V, with current fluctuations recorded for 180 s. Figure 2S in the Supplemental Material [32] shows that the devices are close to the Ohmic regime for the

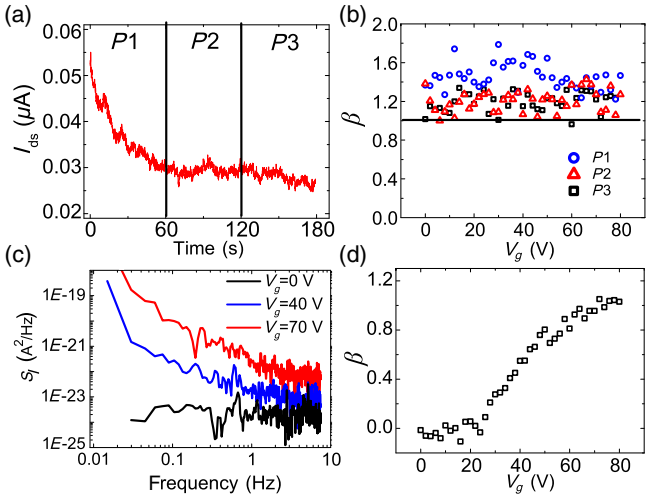

FIG. 3. (a) Drain-source current I_{ds} dependence on time for device III after the gate voltage V_g is steeply swept up by 2 V under dark conditions. The current time series corresponds to a time window of 180 s (determined from the photocurrent exponential-decay time constant), divided into three periods, $P1$, $P2$, and $P3$, of 60 s each. (b) Dependence of the characteristic Hooge parameter β on gate voltage V_g at $P1$, $P2$, and $P3$ for device III under dark conditions. The solid line represents the ideal β value for $1/f$-type LFN. (c) Noise power spectrum measured for device II at $P3$ for different gate voltages under dark conditions. (d) Corresponding gate-voltage dependence of β for device II under dark conditions at $P3$.

full range of gate voltages explored in this work, where S_I is proportional to I_{ds}^2.

Figure 3(a) exhibits the current time-series dependence of device III under dark conditions after a steep sweep of V_g by 2 V, and Fig. 3(b) the corresponding gate dependence for the extracted parameter β at $P1$, $P2$, and $P3$. At the $P3$ interval, the relaxation effects are found to be negligible and indicate that the system is close to equilibrium. Evaluating β as the device operation approaches equilibrium (from $P1$ to $P3$), the exponent β decreases from above 1.5 to closer to 1 [see Fig. 3(b)] without exhibiting a significant gate dependence. The larger β values in the presence of time-dependent relaxation are also observed in off-equilibrium magnetic tunnel junctions near the switching to the antiparallel state [36]. This dependence of the LFN on the period of the current time series is observed in all samples. In order to address possible concerns about spectral leakage along relaxation, we analyze the LFN data only for the periods closest to equilibrium ($P3$).

Focusing henceforth on the current time series period $P3$, device II exhibits a clear dependence of the $S_I(f)$ on the gate voltage. Figure 3(c) shows the noise power spectrum under dark conditions at $V_g = 0$, 40, and 70 V for device II. Plotting $S_I(f)$ in log scale allows us to clearly identify a power dependence on frequency with the Hooge parameter β increasing for higher gate voltages. Figure 3(d) summarizes the gate dependence of β for device II. For $V_g < 20$ V, β is close to 0, changing to $1/f$ noise when $V_g > 40$ V. These results suggest a dependence of the LFN under dark conditions on channel thickness. Still, at sufficiently high gate and close to equilibrium (the $P3$ time window), β is close to 1. However, for devices I and II at the *off* state, β approaches 0, suggesting that a strong random telegraph noise (RTN) overcomes $1/f$-type noise. At higher gates and with an increasing number of layers, the $1/f$ noise contribution overcomes this frequency-independent response at low frequencies [see Figs. 3(b) and 3(d)]. In view of the strong decrease of the defect-assisted recombination times with a decreasing number of layers in MoS_2 [37,38], the absence of the $1/f$ contribution at low gates for devices I and II suggests that dominating generation-recombination processes are leading to a Lorentzian spectrum, where the corresponding noise power spectrum tends to constant noise power values at low frequencies. The observed behavior of β with layer number and electrostatic gating is then likely related to the interplay between two mechanisms in the MoS_2 monolayer to few-layer flakes: the strongly dependent recombination time scales with the number of layers [37,38] and the different intrinsic doping levels of each flake, known to vary strongly with ambient conditions [39].

C. Tuning different noise regimes by photodoping

Two models based on the Hooge relation can be used to describe the origins of the fluctuations in FETs exhibiting $1/f$-type power spectral density. These are the Hooge-mobility-fluctuation [28] and carrier-number-fluctuation models [40]. In the CNF model, $S_I \propto (V_g - V_{th})^{-2}$, with V_{th} being the threshold gate voltage for the opening of the conductance channels. In the HMF model, $S_I \propto N^{-1}$, with N being the carrier density. The low conductivity of MoS_2 FETs places it in the limiting case of weakly conducting regimes, and therefore the CNF model should suit the LFN, where the drain-source current noise power spectral density is expected to show a quadratic dependence on the gate voltage. The HMF model is usually valid for conducting regimes [28].

In the following, we demonstrate that the combined application of gate voltage and laser illumination to our MoS_2 FETs, which affects the carrier density N (Fig. 2), also changes the transport conditions from $1/f$-type noise dominated by CNF to noise dominated by HMF.

Following Ref. [3], we consider overdrive conditions for the analysis, when $|V_g - V_{th}| > 0$, and the carrier density N can be approximated as $N \propto (V_g - V_{th})$. We shall restrict our study to the cases where the power spectrum approximately follows $1/f$ behavior ($0.7 < \beta < 1.5$). In order to reach specific conclusions on the physical processes responsible for the LFN, we plot the gate dependence of the inverse of the normalized noise parameter α for different photodoping conditions [Figs. 4(a), 4(c), and 4(e)].

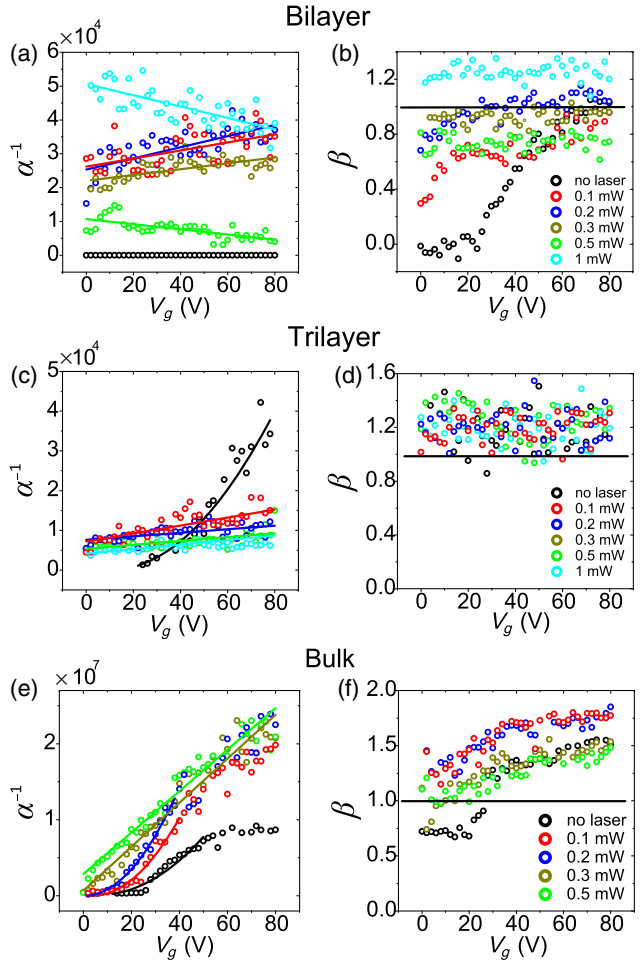

FIG. 4. Gate dependence of α^{-1} and β Hooge parameters for devices II, III, and IV, determined from the LFN measurements under dark conditions and with illumination. Laser power ranges from an absence of illumination (a dark condition referred to as "no laser") to 1 mW. (a),(b) Device II. (c),(d) Device III. (e),(f) Device IV. The solid lines in the α^{-1} plots are fittings to the gate-voltage dependence, and in the β plots represent the ideal β value for a 1/f-type LFN.

Starting with dark conditions, the noise measurements in device I (Fig. 4S of the Supplemental Material [32]) and device II [Fig. 4(b)] suggest that the transition to a sufficiently conducting regime, with $1/f$-type noise, occurs only at gates above 30–40 V. This constrain restricts the inverse noise (α^{-1} vs V_g) analysis to the relatively narrow range of 40 to 80 V, where the corresponding α^{-1} dependence shows a linear trend, indicating HMF as the driving mechanism for the LFN. However, the dispersion of the normalized noise parameters is found to be extremely large for device I (see Fig. 4S of the Supplemental Material [32]). Devices III and IV, on the other hand, exhibit a quadratic dependence of α^{-1} as a function of the gate voltage [see Figs. 4(c) and 4(e), respectively]. This fact—together with the fact that, in the explored gate-voltage range, the devices show $1/f$-type noise (from the β-parameter analysis)—allows us to point to CNF as the underlying physical mechanism driving the LFN [40]. These results allow us to separate the dark-condition LFN in devices I–IV into two categories. More specifically, devices I and II show $1/f$-type noise driven by HMF only above some threshold gate voltage (of about 40 V for device II and 60 V for device I; see Figs. 4S and 5S of the Supplemental Material [32]), with mainly RTN for lower gate voltages, while devices III and IV reveal approximately $1/f$ noise driven by carrier-number fluctuations in the whole range of applied gates from 0 to 80 V (see Fig. 4).

TABLE I. Summary of the LFN for devices I, II, III, and IV, under dark conditions (Dark) and under laser illumination (Light), for two extreme electrostatic-gating regimes (at low gate voltage, but still above overdrive conditions, $V_g \geq V_{th}$, and at the highest gate voltages, $V_g \gg V_{th}$).

	I, II		III, IV	
	$V_g \geq V_{th}$	$V_g \gg V_{th}$	$V_g \geq V_{th}$	$V_g \gg V_{th}$
Dark	RTN	HMF	CNF	CNF
Light	HMF	HMF	HMF	HMF

Under illumination, devices I and II show a linear dependence of $\alpha^{-1} \propto (V_g - V_{th})$. With increased photodoping, the dependence of β on the gate voltage changes from RTN type (seen under dark conditions for gate voltages lower than 40 V) to $1/f$ type across the full gate range, demonstrating how the additional photoconducting channels contribute to LFN dominated by HMF [28]. Interestingly, in device II, for the maximum illumination power of 1 mW, the drain-source current dependence on gate voltage exhibits a decrease for higher gate voltages (Fig. 6S in the Supplemental Material [32] shows this particular case), as well as a strong reduction of the normalized noise power [Fig. 4(a)]. We tentatively attribute this effect to an increase in the recombination rates of the charge carriers, leading to a decrease in conductance and an increase in LFN. For devices III and IV, one clearly observes a transition from a quadratic dependence $\alpha^{-1} \propto (V_g - V_{th})^2$ to a linear dependence $\alpha^{-1} \propto (V_g - V_{th})$, pointing at a crossover from carrier-number fluctuations [40] to fluctuations in the carrier mobility [28], respectively. Note that the LFN data obtained for V_g below V_{th} (i.e., practically in the *off* state) is not used in our fits to extract V_{th} since the McWhorter model is valid only for overdrive conditions where $V_g > V_{th}$. Table I summarizes the several observations under dark and illumination conditions, electrostatic gating (for overdrive conditions), and different layer counts.

The observation of RTN for devices I and II under dark conditions (and low gate voltage), while devices III and IV at the same conditions show CNF, was already discussed in Sec. III B, with the effect originating from the strong dependence of the recombination time scales for different

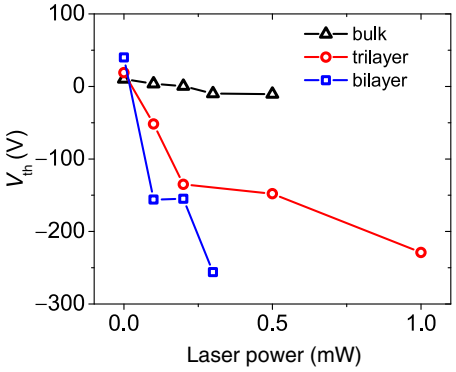

FIG. 5. Estimated threshold voltages for devices II, III, and IV as a function of the laser illumination power. The threshold voltage is determined for a 250-nm-thick SiO_2 dielectric.

layer numbers [37,38]. At low gate voltages, by exciting devices I and II with light, the carrier-density enhancement is enough to drive $1/f$ noise, also of HMF character.

The observed crossover from CNF to HMF in devices III and IV under laser illumination can be understood as a consequence of the percolative character of conductance in the random resistor network of MoS_2 FETs [29]. In this picture, the change in the noise microscopic mechanism driven by light from CNF to HMF reflects the crossing from a regime where transport happens via hopping or tunneling between disconnected metallic puddles at the Fermi level, in the so-called island-and-sea representation of the carrier distribution in the MoS_2 flakes, to a continuum percolation, where instead of a random network of disconnected metallic puddles, there is a continuum electron sea at the Fermi level.

Further analysis of the table allows us to make one additional observation. Under sufficient electron doping (photodoping and high electrostatic gating), all devices show HMF. Together with the fact that electrostatic gating under dark conditions is not enough to drive devices III and IV to HMF LFN (while devices I and II show HMF), this finding strongly suggests that the intrinsic doping levels of devices I and II are higher than they are in devices III and IV. This observation is compatible with a report where Baugher *et al.* observe a higher carrier density for thinner devices [35].

A comparison of the influence of the illumination power on V_{th} (Fig. 5) shows that thinner devices require lower illumination power to achieve significant photodoping, which is reflected by the shift of V_{th} to lower values. V_{th} is determined as the equivalent field-effect electrostatic doping required, with the use of a 250-nm-thick SiO_2 dielectric, to change the MoS_2 device operation from an insulating to a more conductive regime when under the specified illumination conditions (photodoping).

Gathering the several conclusive elements for the dependence of β and α^{-1} on the layer thickness, gating, and laser illumination, the observed effects arise then from a complex interplay between the several electron-doping sources (the intrinsic doping of the flakes, the photodoping, and the electrostatic doping), and the strong decrease of the recombination time scales with a decreasing layer number. RTN noise gives place to $1/f$-type HMF noise in the thinner devices (I and II) under sufficient electron doping, while the thicker devices (III and IV) exhibit mainly $1/f$-type CNF for overdrive conditions. When in the $1/f$-type noise regime, we observe a crossover from CNF to HMF driven by photodoping, where by shining light the discontinuous random resistive network percolates to a continuum electron sea at the Fermi level.

IV. CONCLUSIONS

In this work, we introduce a method to access different LFN regimes in MoS_2 FETs by using photodoping and identify a constraint in the transient decay time window to perform LFN studies. We believe this concept to be applicable in a much wider class of 2D-material-based FETs. Our results confirm the presence of frequency-independent low-frequency generation-recombination noise, previously reported for monolayer MoS_2 FETs studied under environmental conditions [3], attributed to either traps in the SiO_2 substrate or to midgap defect states in MoS_2. For sufficiently thick MoS_2 FETs (above bilayer), electrostatic gating in the dark state reveals $1/f$-type noise driven by carrier-number fluctuations, in agreement with most of the previous reports [4,5,15,19–27]. In these conditions, by using photodoping with reasonably small laser powers, we are able to tune the origin of the conductance fluctuations from carrier-number fluctuations to carrier mobility fluctuations. Our findings introduce, then, a versatile approach for investigating LFN in 2D vdW-based FETs, paving the way to overcome LFN limitations of TMD-based photodetectors and transistors.

ACKNOWLEDGMENTS

The work in Madrid was supported by Spanish MINECO (Grant No. MAT2015-66000-P) and the Comunidad de Madrid through NANOFRONTMAG-CM (Grant No. S2013/MIT-2850). The work in CIC nanoGUNE was supported by the European Union 7th Framework Programme under the Marie Curie Actions (Grant No. 607904-13-SPINOGRAPH), by the Spanish MINECO under Project No. MAT2015-65159-R, and by the Basque Government under Project No. PC2015-1-01.

I. M. and M. R. contributed equally to this work.

[1] A. Ambrosetti, N. Ferri, R. A. DiStasio, Jr., and A. Tkatchenko, Wavelike charge density fluctuations and van der Waals interactions at the nanoscale, Science **351**, 1171 (2016).

[2] A. Balandin, Low-frequency 1/f noise in graphene devices, Nat. Nanotechnol. **8**, 549 (2013).
[3] V. K. Sangwan, N. H. Arnold, D. Jariwala, T. J. Marks, L. J. Lauhon, and M. C. Hersam, Low-frequency electronic noise in single-layer MoS_2 transistors, Nano Lett. **13**, 4351 (2013).
[4] J. Renteria, R. Samnakay, S. L. Rumyantsev, C. Jiang, P. Goli, M. S. Shur, and A. A. Balandin, Low-frequency 1/f noise in MoS_2 transistors: Relative contributions of the channel and contacts, Appl. Phys. Lett. **104**, 153104 (2014).
[5] H.-J. Kwon, H. Kang, J. Jang, S. Kim, and C. P. Grigoropoulos, Analysis of flicker noise in two-dimensional multilayer MoS_2 transistors, Appl. Phys. Lett. **104**, 083110 (2014).
[6] I.-T. Cho, J. I. Kim, Y. Hong, J. Roh, H. Shin, G. W. Woo Baek, C. Lee, B. H. Hong, S. H. Jin, and J.-H. Lee, Low frequency noise characteristics in multilayer WSe_2 field effect transistor, Appl. Phys. Lett. **106**, 023504 (2015).
[7] B. Radisavljevic, A. Radenovic, J. Brivio, V. Giacometti, and A. Kis, Single-layer MoS_2 transistors, Nat. Nanotechnol. **6**, 147 (2011).
[8] D. Sarkar, X. Xie, W. Liu, W. Cao, J. Kang, Y. Gong, S. Kraemer, P. M. Ajayan, and K. Banerjee, A subthermionic tunnel field-effect transistor with an atomically thin channel, Nature (London) **526**, 91 (2015).
[9] H. Wang, L. Yu, Y.-H. Lee, Y. Shi, A. Hsu, M. L. Chin, L. J. Li, M. Dubey, J. Kong, and T. Palacios, Integrated circuits based on bilayer MoS_2 transistors, Nano Lett. **12**, 4674 (2012).
[10] S. Kim, A. Konar, W.-S. Hwang, J. H. Lee, J. Lee, J. Yang, C. Jung, H. Kim, J.-B. Yoo, and J.-Y Choi, High-mobility and low-power thin-film transistors based on multilayer MoS_2 crystals, Nat. Commun. **3**, 1011 (2012).
[11] M. M. Furchi, A. Pospischil, F. Libisch, J. Burgdörfer, and T. Mueller, Photovoltaic effect in an electrically tunable van der Waals heterojunction, Nano Lett. **14**, 4785 (2014).
[12] S. Memaran, N. R. Pradhan, Z. Lu, D. Rhodes, J. Ludwig, Q. Zhou, O. Ogunsolu, P. M. Ajayan, D. Smirnov, A. I. Fernández-Dominguez, F. J. García-Vidal, and L. Balicas, Pronounced photovoltaic response from multilayered transition-metal dichalcogenides PN-junctions, Nano Lett. **15**, 7532 (2015).
[13] M. Buscema, J. O. Island, D. J. Groenendijk, S. I. Blanter, G. A. Steele, H. S. J. van der Zant, and A. Castellanos-Gomez, Photocurrent generation with two-dimensional van der Waals semiconductors, Chem. Soc. Rev. **44**, 3691 (2015).
[14] F. K. Perkins, A. L. Firedman, E. Cobas, P. M. Campbell, G. G. Jernigan, and B. T. Jonker, Chemical vapor sensing with mono layer MoS_2, Nano Lett. **13**, 668 (2013).
[15] Y.-F. Lin, Y. Xu, C.-Y. Lin, Y.-W. Suen, M. Yamamoto, S. Makaharai, K. Ueno, and K. Tsukagoshi, Origin of noise in layered $MoTe_2$ transistors and its possible use for environmental sensors, Adv. Mater. **27**, 6612 (2015).
[16] D. J. Late, B. Liu, H. S. S. R. Matte, V. P. Dravid, and C. N. R. Rao, Hysteresis in single-layer MoS_2 field effect transistors, ACS Nano **6**, 5635 (2012).
[17] Y. Guo, X. Wei, J. Shu, B. Liu, J. Yin, C. Guan, Y. Han, S. Gao, and Q. Chen, Charge trapping at the MoS_2-SiO_2 interface and its effects on the characteristics of MoS_2 metal-oxide-semiconductor field effect transistors, Appl. Phys. Lett. **106**, 103109 (2015).
[18] Y.-C. Wu, C.-H. Liu, S.-Y. Chen, F.-Y. Shih, P.-H. Ho, C.-W. Chen, C.-T. Liang, and W.-H. Wang, Extrinsic origin of persistent photoconductivity in monolayer MoS_2 field effect transistors, Sci. Rep. **5**, 11472 (2015).
[19] M.-K. Joo, Y. Yun, S. Yun, Y. H. Lee, and D. Suh, Strong Coulomb scattering effects on low frequency noise in monolayer WS_2 field-effect transistors, Appl. Phys. Lett. **109**, 153102 (2016).
[20] S.-P. Ko, J. M. Shin, Y. J. Kim, H. K. Jang, J. E. Jin, M. Shin, Y. K. Kim, and G. T. Kim, Current fluctuation of electron and hole carriers in multilayer WSe_2 field effect transistors, Appl. Phys. Lett. **107**, 242102 (2015).
[21] S. R. Das, J. Kwon, A. Prakash, C. J. Delker, S. Das, and D. B. Janes, Low-frequency noise in $MoSe_2$ field effect transistors, Appl. Phys. Lett. **106**, 083507 (2015).
[22] D. Sharma, M. Amani, A. Motayed, P. B. Shah, A. G. Birdwell, S. Najmaei, P. M. Ajayan, J. Lou, M. Dubey, Q. Li, and A. V. Davydov, Electrical transport and low-frequency noise in chemical vapor deposited single-layer MoS_2 devices, Nanotechnology **25**, 155702 (2014).
[23] S. Ghatak, S. Mukherjee, M. Jain, D. D. Sarma, and A. Ghosh, Microscopic origin of low frequency noise in MoS_2 field-effect transistors, APL Mater. **2**, 092515 (2014).
[24] X. Xie, D. Sarkar, W. Liu, J. Kang, O. Marinov, M. J. Deen, and K. Banerjee, Low-frequency noise in bilayer MoS_2 transistor, ACS Nano **8**, 5633 (2014).
[25] J. Na, M.-K. Joo, M. Shin, J. Huh, J.-S. Kim, M. Piao, J.-E. Jin, H.-K. Jang, H. J. Cho, J. H. Shim, and G.-T. Kim, Low-frequency noise in multilayer MoS_2 field-effect transistors: The effect of high-k passivation, Nanoscale **6**, 433 (2014).
[26] D. Sharma, A. Motayed, P. B. Shah, M. Amani, M. Georgieva, A. G. Birdwell, M. Dubey, Q. Li, and A. V. Davydov, Transfer characteristics and low-frequency noise in single-and multi-layer MoS_2 field-effect transistors, Appl. Phys. Lett. **107**, 162102 (2015).
[27] S. L. Rumyantsev, C. Jiang, R. Samnakay, M. S. Shur, and A. A. Balandin, $1/f$ noise characteristics of MoS_2 thin-film transistors: Comparison of single and multilayer structures, IEEE Electron Device Lett. **36**, 517 (2015).
[28] F. N. Hooge, $1/f$ noise is no surface effect, Phys. Lett. **29A**, 139 (1969).
[29] T. Paul, S. Ghatak, and A. Ghosh, Percolative switching in transition metal dichalcogenide field-effect transistors at room temperature, Nanotechnology **27**, 125706 (2016).
[30] A. Castellanos-Gomez, M. Buscema, R. Molenaar, V. Singh, L. Janssen, H. S. J. van der Zant, and G. A. Steele, Deterministic transfer of two-dimensional materials by all-dry viscoelastic stamping, 2D Mater. **1**, 011002 (2014).
[31] H. Li, Q. Zhang, C. C. R. Yap, B. K. Tay, T. H. T. Edwin, A. Oliver, and D. Baillargeat, From bulk to monolayer MoS_2: Evolution of Raman scattering, Adv. Funct. Mater. **22**, 1385 (2012).
[32] See Supplemental Material at http://link.aps.org/supplemental/10.1103/PhysRevApplied.7.034034 for the transfer curves of devices I and IV; the pulsed photocurrent response as a function of the MoS_2 thickness; a noise and photocurrent characterization of the single-layer MoS_2 FET; and the photocurrent response for devices I–IV at different laser powers.

[33] M. Fontana, T. Deppe, A. K. Boyd, M. Rinzan, A. Y. Liu, M. Paranjape, and P. Barbara, Electron-hole transport and photovoltaic effect in gated MoS_2 Schottky junctions, Sci. Rep. **3**, 1634 (2013).

[34] A. Allain, J. Kang, K. Banerjee, and A. Kis, Electrical contacts to two-dimensional semiconductors, Nat. Mater. **14**, 1195 (2015).

[35] B. W. H. Baugher, H. O. H. Churchill, Y. Yang, and P. Jarillo-Herrero, Intrinsic electronic transport properties of high-quality monolayer and bilayer MoS_2, Nano Lett. **13**, 4212 (2013).

[36] R. Guerrero, F. G. Aliev, R. Villar, R. Ortega-Hertogs, W. K. Park, and J. S. Moodera, Low frequency noise in $Co/Al_2O_3\langle\delta(Fe)\rangle/Ni_{80}Fe_{20}$ magnetic tunnel junctions, J. Phys. D **35**, 1761 (2002).

[37] H. Wang, C. Zhang, and F. Rana, Ultrafast dynamics of defect-assisted electron-hole recombination in monolayer MoS_2, Nano Lett. **15**, 339 (2015).

[38] H. Wang, C. Zhang, and F. Rana, Surface recombination limited lifetimes of photoexcited carriers in few-layer transition metal dichalcogenide MoS_2, Nano Lett. **15**, 8204 (2015).

[39] H.-J. Kwon, J. Jang, S. Kim, V. Subramanian, and C. P. Grigoropoulos, Electrical characteristics of multilayer MoS_2 transistors at real operating temperatures with different ambient conditions, Appl. Phys. Lett. **105**, 152105 (2014).

[40] E. Simoen and C. Claeys, On the flicker noise in submicron silicon MOSFETs, Solid State Electron. **43**, 865 (1999).